

Article

Optical and Transport Properties of Ni-MoS₂

Tsung-Shine Ko, Cheng-Ching Huang and Der-Yuh Lin *

Department of Electronic Engineering, National Changhua University of Education, No.2, Shi-Da Road, Changhua City, Changhua County 500, Taiwan; tsko@cc.ncue.edu.tw (T.-S.K.); bq97001@hust.edu.tw (C.-C.H.)

* Correspondence: dylin@cc.ncue.edu.tw; Tel.: +886-4-7232105 (ext. 8357)

Academic Editor: Andres Castellanos-Gomez

Received: 7 June 2016; Accepted: 8 August 2016; Published: 12 August 2016

Abstract: In this paper, MoS₂ and Ni-MoS₂ crystal layers were fabricated by the chemical vapor transport method with iodine as the transport agent. Two direct band edge transitions of excitons at 1.9 and 2.1 eV were observed successfully for both MoS₂ and Ni-MoS₂ samples using temperature-dependent optical reflectance (R) measurement. Hall effect measurements were carried out to analyze the transport behavior of carriers in MoS₂ and Ni-MoS₂, which indicate that the Ni-MoS₂ sample is *n*-type and has a higher resistance and lower mobility than the MoS₂ sample has. A photoconductivity spectrum was performed which shows an additional Ni doping level existing at 1.2 eV and a higher photocurrent generating only for Ni-MoS₂. The differences between MoS₂ and Ni-MoS₂ could be attributed to the effect of Ni atoms causing small lattice imperfections to form trap states around 1.2 eV. The temperature-dependent conductivity shows the presence of two shallow levels with activation energies (84 and 6.7 meV in MoS₂; 57 and 6.5 meV in Ni-MoS₂). Therefore, the Ni doping level leads to high resistance, low mobility and small activation energies. A series of experimental results could provide useful guidance for the fabrication of optoelectronic devices using MoS₂ structures.

Keywords: reflectance; Hall effect; photoconductivity; Ni dopants; MoS₂

1. Introduction

In recent years, transition metal dichalcogenides (TMDCs) have attracted great attention owing to their two-dimensional layer structure which is analogous to graphene [1,2]. As a member of the TMDC family, molybdenum disulfide (MoS₂) with a direct bandgap is complementary to the graphene and suggests a great potential for logic devices, integrated circuits, and optoelectronics [3–6]. Therefore, MoS₂ is rallied up as a finite-energy-bandgap alternative to graphene in advanced electronic and photonic device applications [7–11]. Several interesting properties of MoS₂ have been also studied in terms of the optical properties and electrical structure. For example, Ayari et al. reported there is a transition for MoS₂ from an indirect bandgap in the bulk to a direct gap in the few-layer structures [12], which would be desirable and beneficial for TMDC transistor development. Kadantsev et al. investigated the electronic structure of a single MoS₂ monolayer using first-principles calculations [13], and their results point out that a single MoS₂ monolayer is a direct K to K bandgap semiconductor. Howell et al. studied discontinuous characteristics in energy bands that exist at the interface of monolayer and multilayer thin films [14]. Amani et al. carried out a detailed study to understand the behavior of the electrical performance of monolayer MoS₂ field-effect transistors using the chemical vapor deposition method [15]. Furthermore, Kenneth et al. demonstrated near-field electrical detection of silver nanowire plasmons with the atomically thin semiconductor molybdenum disulfide [16]. In spite of many relevant MoS₂ characteristics being determined, so far little is known about the properties of the doping categories and their effect on optical and electrical characteristics in terms of whether MoS₂ is a monolayer or bulk. A stable *p*-type MoS₂ is important for TMDC device applications

and has been performed by Nb doping against the native *n*-type propensity in unintentionally doped MoS₂ [17]. In that study a stable *p*-type conduction with a degenerate hole density of $\sim 3 \times 10^{19} \text{ cm}^{-3}$ in MoS₂ has been demonstrated. Furthermore, Guha et al. pointed out that natural MoS₂ was *p*-type in the early period [18]. Nevertheless, most studies revealed that MoS₂ ought to be *n*-type [19,20]. Among these studies on dopants, little information has been published concerning the material and physical properties for Ni-MoS₂ thin film. Herein, we have also undertaken a series of experiments to analyze the optical and electrical properties of pure MoS₂ and Ni-MoS₂.

In this paper, both MoS₂ samples with and without the Ni dopant were prepared by the chemical vapor transport (CVT) method. In terms of optical and electrical properties, reflectance (R), transmittance, photoconductivity (PC), and Hall effect measurements were carried out for both samples. A series of experiments results confirmed the Ni dopant effect on fundamental material properties which could provide guidance for further electronic and optoelectronic devices of MoS₂.

2. Experimental Details

The MoS₂ single crystals were grown by the CVT method for this study, using I₂ as a transporting agent. The iodine transport agent and the elements including Mo (99.99%), S (99.99%) and Ni (99.99%) were used for the crystal growth. The molar ratio of Mo/S is 1:2. The intentional doping concentration of Ni is 0.5%. Afterward, whole reactants were placed in quartz tubes which were evacuated to 2×10^{-5} torr and sealed. For growing the crystals, the quartz tube was placed in a three-zone furnace and grown at 1000 °C for 720 h. In order to obtain an optimal diffusion gradient for crystal growth, the temperature gradient was adjusted at 1050 to 935 °C. We carried out electron spectroscopy for chemical analysis (ESCA) for Ni-MoS₂ to confirm existence of elements like nickel or iodine. Figure 1a,b shows the ESCA results which indicate our Ni-MoS₂ actually has Ni atoms with low percentage of 0.2%. No iodine was detected for both samples using ESCA analysis which provides evidence that probably only a few iodine atoms in both samples. The sample surface was observed using an homemade optical microscope (OM) system. A 150 W Xenon lamp equipped with a PTI 0.25 m monochromator was used to provide monochromatic light which was chopped by a mechanical chopper at frequency of 200 Hz for R measurement. The monochromatic light reflected from the sample surface. Consequently the light was collected by lens, detected by a photomultiplier tube (PMT) and recorded by a lock-in amplifier. Meanwhile, a closed-cycle cryostat was utilized to control the temperature changing from 20 to 300 K for R experiment. The same light source and similar setup were also employed in PC and transmittance experiments. As for PC measurements, the sample was connected in series to a resistor (10 kΩ) and a constant voltage (1 V) to complete a circuit loop. The frequency of probe light was chopped and fixed 7 Hz. We utilized van der Pauw method to carry out Hall effect measurement at room temperature. The electrical properties of MoS₂ and Ni-MoS₂ were investigated including carrier concentration, resistance and mobility. Since the shape of sample is irregular, the four contacts were made to sides in square shape located at the edges of the sample with the same distance between each contact [21]. The temperature-dependent I-V measurements from 20 to 300 K were also carried out in a closed-cycle He-cryostat for temperature conductivity analysis. The samples were illuminated with monochromatic light of 1.2 eV filtered from a xenon lamp.

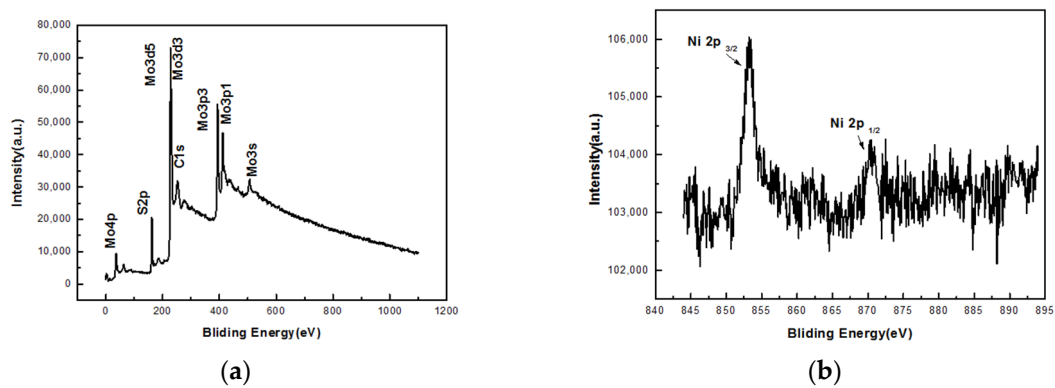


Figure 1. Electron spectroscopy for chemical analysis (ESCA) results of (a) full spectrum and (b) high resolution in Ni region for Ni-MoS₂.

3. Results and Discussion

The samples were formed with many stacked layers after growth. The thickness of the layered MoS₂ crystal is about 20 μm . The three-dimensional crystal is formed by stacking the two-dimensional MoS₂ sheets. Since there is the interaction of a weak van der Waals force providing a natural cleavage plane of the crystal between two adjacent MoS₂ sheets [22], it would be easy to separate the samples into thin specimens with a smooth surface. The OM images of MoS₂ and Ni-MoS₂ are presented in Figure 2. According to previous literature, the optical micrograph image of the surface of 2H MoS₂ may show a hexagonal shape, while that of 3R MoS₂ may show a triangular shape [23,24]. In our case, both images show the feature with hexagonal corners ($\gamma = 120$ degrees) on the surface, indicating that the MoS₂ samples are 2H single crystals. The smooth surfaces of MoS₂ are beneficial for performing the R measurements [25].

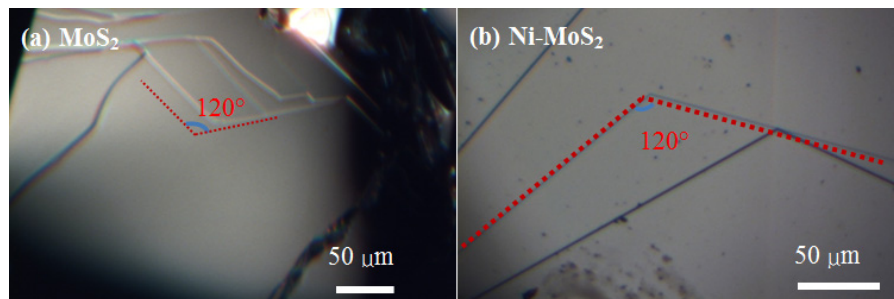


Figure 2. (Optical microscope) OM images of (a) MoS₂ and (b) Ni-MoS₂ under 30 \times magnification.

In order to understand exciton behavior in MoS₂ and Ni-MoS₂, temperature-dependent R spectra were carried out at a temperature range of 20 to 300 K for both MoS₂ and Ni-MoS₂ samples. The results of the R spectra of the MoS₂ and Ni-MoS₂ indicate two main resonance features existing in each spectrum for both samples, as Figure 3 shows. We analyzed these spectra using the below Equation (1) proposed by Korona et al. [26]

$$R(\nu) = R_0 + R_x \text{Re} \left[\frac{h\nu_x - h\nu + i\Gamma_x}{\Gamma_x^2 + (h\nu - h\nu_x)^2} \right] e^{i\Theta} \quad (1)$$

where R_0 is the background, R_x is the intensity, $h\nu_x$ is the photon energy, Γ_x is the broadening parameter and Θ is the phase. Afterward, two obvious peaks at 1.83 and 2.02 eV were obtained and denoted as A and B at 300 K, respectively. The energy difference between A and B excitonic transitions is 0.15 eV [23]. Furthermore, the values of features A and B are a little lower than those observed in the absorption

peaks and photoluminescence peaks of atomically thin MoS₂ samples [9], which could explain these two features arising from direct bandgap transitions between the maxima of split valance bands (v1 and v2) and the minimum of the conduction band (c1). The valance band was split due to the combined effects including the interlayer and spin-orbit coupling [27]. Both features are gradually shifted to the slight highly 1.91 and 2.11 eV, respectively, when the temperature is ramped down to 20 K due to less thermal activation. In addition, both direct bandgap transitions A and B in the R spectra of the Ni-MoS₂ are very close to that of the MoS₂ under different temperatures. Therefore, this result could indirectly reflect that the MoS₂ crystal structure did not suffer from much distortion even though Ni atoms were doped. On the other hand, the interference feature could be found only in the R spectrum of Ni-MoS₂. This could be attributed to the poor surface roughness of the MoS₂ we picked up for measurement.

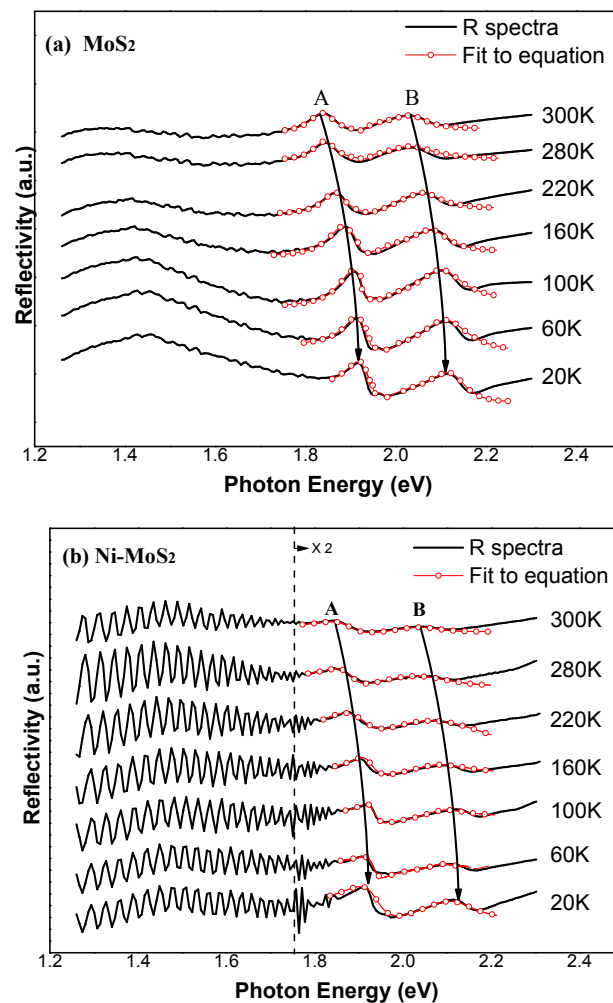


Figure 3. Temperature-dependent reflection spectra of (a) MoS₂ and (b) Ni-MoS₂ samples.

Here we adopted the Varshni equation, $E_g(T) = E_g(0) - (\alpha T^2 / (T + \beta))$, to describe the bandgap reduction with the temperature [28]. The constant α is related to the electron-phonon and β is related to the Debye temperature. The spectral shift of the A and B features with the energy is depicted in Figure 4. Furthermore, another analysis method was also considered which was proposed by O'Donnell and Chen [29]. The empirical expression is shown as below in Equation (2).

$$E_i^{ex}(T) = E_i^{ex}(0) - S \langle \hbar\Omega \rangle \left[\coth \frac{\langle \hbar\Omega \rangle}{2KT} - 1 \right] \quad (2)$$

where $E_i^{ex}(0)$ is the band gap at 0 K, S is a dimensionless coupling constant, and $\hbar\Omega$ is an average phonon energy. By fitting the Varshni equation (red line) and O'Donnell's empirical expression (blue line), the temperature dependence of the A and B transitions could be obtained. The fitted parameters are listed in Table 1. The trend and fitted parameters shown here have a reasonable consistency with similar results of reflection of the MoS₂ as proposed by Ho et al. [30]. Therefore, the temperature shift of excitonic-transition energies could be attributed to both the lattice variations and interactions with relevant acoustic and optical phonons.

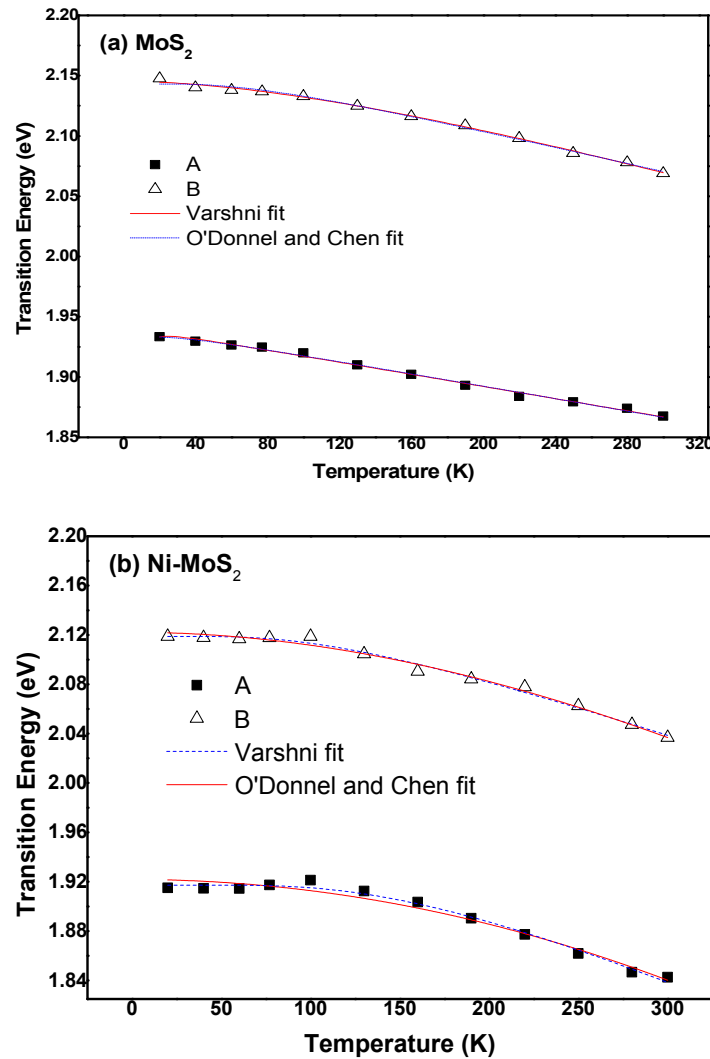


Figure 4. Temperature-dependent excitonic transition energies of (a) MoS₂ and (b) Ni-MoS₂ samples.

Table 1. Values of fitting parameters of the Varshni equation and the expression proposed by O'Donnell and Chen [29], which describe the temperature dependence of the transition energies of MoS₂ and Ni-MoS₂.

| Material | Feature | $E_i^{ex}(0)$ (eV) | A (meV/K) | B (K) | S | $\langle\hbar\Omega\rangle$ (meV) |
|---------------------|---------|--------------------|------------------|-----------------|------------------|-----------------------------------|
| MoS ₂ | A | 1.940 ± 0.005 | 0.353 ± 0.05 | 125.2 ± 100 | 2.033 ± 0.1 | 13.1 ± 3 |
| | B | 2.130 ± 0.005 | 0.355 ± 0.05 | 252.2 ± 100 | 2.007 ± 0.1 | 28.5 ± 3 |
| Ni-MoS ₂ | A | 1.918 ± 0.005 | 0.582 ± 0.05 | 399.7 ± 100 | 2.271 ± 0.05 | 20.38 ± 3 |
| | B | 2.118 ± 0.005 | 0.517 ± 0.05 | 236.2 ± 100 | 2.215 ± 0.05 | 14.67 ± 3 |

Room-temperature Hall effect measurements were performed for MoS₂ and Ni-MoS₂. The relevant results are shown in Table 2. The Hall effect measurement results indicate that the carrier types of the MoS₂ and Ni-MoS₂ samples are *n*-type. The mobilities of the MoS₂ and Ni-MoS₂ samples are 78.51 and 1.87 cm²V⁻¹s⁻¹, respectively. The resistance was increased about 40 times when Ni was doped into MoS₂. Although the Hall effect measurements also indicate that the Ni-MoS₂ possesses a similar carrier density of $\sim 1.1 \times 10^{13}$ cm⁻² as MoS₂ does, Ni-MoS₂ still has a lower mobility and higher resistance than the undoped MoS₂ has. These results confirm that Ni atoms could not contribute additional electrons or electron holes in MoS₂. On the contrary, these Ni atoms seem to form defects/traps to obstruct electron flows. Meanwhile, Ni dopants produced a band tailing effect due to slight crystal distortion, resulting in the A and B peaks for Ni-MoS₂ being slightly lower than those for MoS₂.

Table 2. The results of room-temperature Hall effect measurements for MoS₂ and Ni-MoS₂.

| Sample | MoS ₂ | Ni-MoS ₂ |
|-------------------------------------|------------------------|------------------------|
| Type | <i>n</i> | <i>n</i> |
| Resistance (Ω) | 6733 | 283188 |
| Carrier density (cm ⁻²) | 1.102×10^{13} | 1.183×10^{13} |
| Mobility(cm ² /V·s) | 78.5089 | 1.86593 |

We implemented PC measurements using a DC bias of 1 V, which records the alternating current induced by the ON/OFF illumination controlled by a mechanical chopper at a frequency of 7 Hz at different photo energies. Meanwhile, transmittance was also carried out at 20 K for comparison. The low temperature PC and transmittance spectrum measured at 20 K are shown in Figure 5. PC results indicate that the main peaks A and B were also observed for both MoS₂ and Ni-MoS₂ samples, which is consistent with previous R measurements. In additions, there is an extra signal that occurs at 1.2 eV, indicated by D. However, no obvious peak could be found at 1.2 eV for the MoS₂. For the Ni-MoS₂ sample, this peak D could be attributed to Ni dopants that induce an additional Ni doping level, providing a different transition path of carriers. In addition, the whole PC spectrum of Ni-MoS₂ is wider than that of undoped MoS₂, which leads to ambiguous A and B positions in the PC spectrum of Ni-MoS₂. Since Ni dopants not only introduce a doping level but also some impurities or defects that cause additional deep levels in the forbidden band, these multi-levels probably result in an obvious and wide width in the PC spectrum of Ni-MoS₂. As for the transmittance results, we carried out transmission experiments for samples after exfoliating them several times. The normalized transmission results for MoS₂ and Ni-MoS₂ have been also included in Figure 5. The ratio of normalized transmission gradually decreased from 1.3 to 1.9 eV due to absorption. However, a low transmission still could be found above 1.9 eV, which could be attributed to some tiny cracks. These cracks were probably produced during the exfoliating process and led to samples that could not absorb the whole photoenergy. In contrast, there is no doping state in the PC spectrum except for both clear A and B excitons, which is consistent with the reflectance results. Since these electrons in the doping state transit to the conduction band, it is worth noting that the photocurrent has been enhanced up to several tens of times and the response wavelength has also been extended when Ni is doped in MoS₂. This result indicates that the doping is a good way to improve their applications in light responsibility for solar cells and photo detectors.

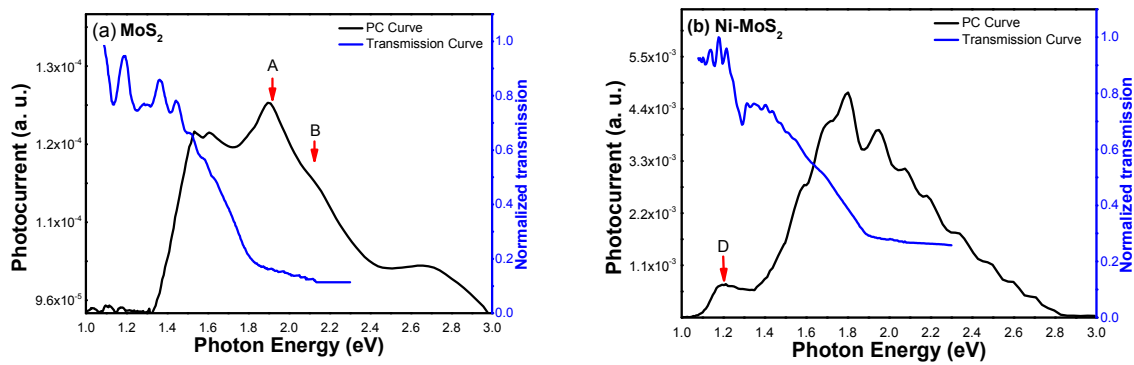


Figure 5. Photoconductivity (PC) and normalized transmission results of MoS₂ and Ni-MoS₂ samples. A peak at 1.2 eV in the PC spectrum was observed only for Ni-MoS₂.

In order to understand the temperature dependence and the activation energy of the Ni-induced defect in MoS₂, we carried out temperature-dependent I-V measurements and analyzed the temperature-dependent conductivity of MoS₂ and Ni-MoS₂ for the calculation of activation energy. The samples were illuminated with a monochromatic light of 1.2 eV filtered from a xenon lamp. A typical semiconducting transport behavior is observed for both samples from the conductivity (σ)-T plot shown in Figure 6. The σ decreases gradually while lowering the temperature from 300 to 20 K. The inset in Figure 6 shows the Arrhenius plot of both samples. It is possible to obtain information about the activation energy by analyzing the experimental data on the basis of the following relation (3):

$$\sigma = \sigma_0 \times \exp(-E_a/kT) \tag{3}$$

where σ_0 is the preexponential factor, E_a is the activation energy and k is the Boltzmann constant. For MoS₂, two different slopes can roughly be differentiated and the corresponding values of activation energy E_a are calculated as $E_a^1 = 84$ meV and $E_a^2 = 6.7$ meV, respectively. On the other hand, activation energy E_a of Ni-MoS₂ is 57 meV for E_a^1 and 6.5 meV for E_a^2 . These results indicate the presence of shallower donors in Ni-MoS₂. In principle, smaller E_a values in Ni-MoS₂ could be attributed to Ni-induced donor defects or related impurities.

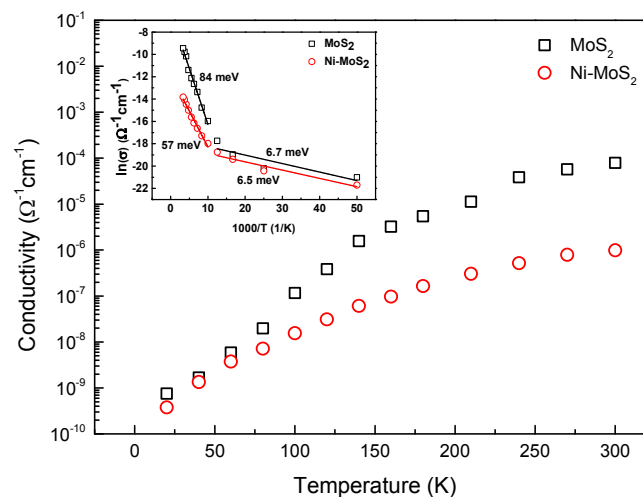


Figure 6. The calculated conductivity versus temperature and corresponding Arrhenius plot (the inset) of the MoS₂ and Ni-MoS₂.

4. Conclusions

In conclusion, both MoS₂ and Ni-MoS₂ samples were grown by the CVT method. Two direct transitions and one indirect transition for both samples were observed successfully via R spectra analysis. Although the Hall effect measurements indicate that MoS₂ and Ni-MoS₂ possesses a similar carrier concentration, the Ni-MoS₂ still has a lower mobility and higher resistance than the undoped MoS₂ has. The characteristics of the *n*-type carrier were confirmed for both samples simultaneously. PC measurements reveal Ni dopants introducing an additional deep Ni doping level existing at 1.2 eV for the Ni-MoS₂ sample which also enhanced the photocurrent. In addition, two shallow activation energies ($E_a^1 = 84$ meV and $E_a^2 = 6.7$ meV) in MoS₂ and ($E_a^1 = 57$ meV and $E_a^2 = 6.5$ meV) Ni-MoS₂ have been defined in this study. Smaller E_a values in Ni-MoS₂ could be attributed to Ni-induced donor defects or a related impurity. These results confirm Ni atoms which could not contribute additional electrons or electron holes in MoS₂. Instead, Ni dopants in MoS₂ would introduce an additional deep level at 1.2 eV causing high resistance and low mobility.

Acknowledgments: This study was supported by the Ministry of Science and Technology of Taiwan, Republic of China under Contracts MOST 104-2221-E-018-017 and MOST 104-2112-M-018-004.

Author Contributions: D.-Y.L. conceived and designed the experiments; C.-C.H. performed the experiments; T.-S.K. and D.-Y.L. analyzed the data; D.-Y.L. contributed reagents/materials/analysis tools; T.-S.K. and D.-Y.L. wrote the paper.

Conflicts of Interest: The authors declare no conflict of interest.

References

1. Balandin, A.A.; Ghosh, S.; Bao, W.; Calizo, I.; Teweldebrhan, D.; Miao, F.; Lau, C.N. Deoxygenation of exfoliated graphite oxide under alkaline conditions: A green route to graphene preparation. *Nano Lett.* **2008**, *8*, 902–907. [[CrossRef](#)] [[PubMed](#)]
2. Mayorov, A.S.; Gorbachev, R.V.; Morozov, S.V.; Britnell, L.; Jalil, R.; Ponomarenko, L.A.; Blake, P.; Novoselov, K.S.; Watanabe, K.; Taniguchi, T.; et al. Micrometer-scale ballistic transport in encapsulated graphene at room temperature. *Nano Lett.* **2011**, *11*, 2396–2399. [[CrossRef](#)] [[PubMed](#)]
3. Gourmelon, E.; Lignier, O.; Hadouda, H.; Couturier, G.; Bernede, J.C.; Tedd, J.; Pouzed, J.; Salardenne, J. Solar Energy materials and solar cells. *Sol. Energy Mater. Sol. Cells* **1997**, *46*, 115–121. [[CrossRef](#)]
4. Ho, W.K.; Yu, J.C.; Lin, J.; Yu, J.G.; Li, P.S. Preparation and photocatalytic behavior of MoS₂ and WS₂ nanocluster sensitized TiO₂. *Langmuir* **2004**, *20*, 5865–5869. [[CrossRef](#)] [[PubMed](#)]
5. Wu, C.C.; Jariwala, D.; Sangwan, V.K.; Marks, T.J.; Hersam, M.C.; Lauhon, L.J. Elucidating the photoresponse of ultrathin MoS₂ field-effect transistors by scanning photocurrent microscopy. *J. Phys. Chem. Lett.* **2013**, *4*, 2508–2513. [[CrossRef](#)]
6. Yamaguchi, H.; Blancon, J.C.; Koppera, R.; Lei, S.; Najmaei, S.; Mangum, B.D.; Gupta, G.; Ajayan, P.M.; Lou, J.; Chhowalla, M.; et al. Spatially Resolved photoexcited charge-carrier dynamics in phase-engineered monolayer MoS₂. *ACS Nano* **2015**, *9*, 840–849. [[CrossRef](#)] [[PubMed](#)]
7. Novoselov, K.S.; Geim, A.K.; Morozov, S.V.; Jiang, D.; Katsneison, M.I.; Grigorieva, I.V.; Dubonos, S.V.; Firsov, A.A. Two-dimensional gas of massless Dirac fermions in graphene. *Nature* **2005**, *438*, 197–200. [[CrossRef](#)] [[PubMed](#)]
8. Zhang, Y.; Tan, Y.W.; Stormer, H.L.; Kim, P. Experimental observation of the quantum Hall effect and Berry's phase in graphene. *Nature* **2005**, *438*, 201–204. [[CrossRef](#)] [[PubMed](#)]
9. Qiu, H.; Pan, L.; Yao, Z.; Li, J.; Shi, Y.; Wang, X. Electrical characterization of back-gated bi-layer MoS₂ field-effect transistors and the effect of ambient on their performances. *Appl. Phys. Lett.* **2012**, *100*, 123104–123106. [[CrossRef](#)]
10. Radisavljevic, B.; Radenovic, A.; Brivio, J.; Giacometti, V.; Kis, A. Single-layer MoS₂ transistors. *Nat. Nano Technol.* **2011**, *6*, 147–150. [[CrossRef](#)] [[PubMed](#)]
11. Jariwala, D.; Sangwan, V.K.; Lauhon, L.J.; Marks, T.J.; Hersam, M.C. Emerging device applications for semiconducting two-dimensional transition metal dichalcogenides. *ACS Nano* **2014**, *8*, 1102–1120. [[CrossRef](#)] [[PubMed](#)]

12. Ayari, A.; Cobas, E.; Ogundadegbe, O.; Fuhrer, M.S. Two-dimensional nanosheets produced by liquid exfoliation of layered materials. *J. Appl. Phys.* **2007**, *101*, 014507–014511. [[CrossRef](#)]
13. Kadantsev, E.S.; Hawrylak, P. Electronic structure of a single MoS₂ monolayer. *Solid State Commun.* **2012**, *153*, 909–913. [[CrossRef](#)]
14. Howell, S.L.; Jariwala, D.; Wu, C.C.; Chen, K.S.; Sangwan, V.K.; Kang, J.; Marks, T.J.; Hersam, M.C.; Lauhon, L.J. Investigation of band-offsets at monolayer–multilayer MoS₂ junctions by scanning photocurrent microscopy. *Nano Lett.* **2015**, *15*, 2278–2284. [[CrossRef](#)] [[PubMed](#)]
15. Matthew, M.A.; Chin, L.; Birdwell, A.G.; O'Regan, T.P.; Najmaei, S.; Liu, Z.; Ajayan, P.M.; Lou, J.; Dubey, M. Electrical characterization of back-gated bi-layer MoS₂ field-effect transistors and the effect of ambient on their performances. *Appl. Phys. Lett.* **2013**, *102*, 193107–193109.
16. Goodfellow, K.M.; Chakraborty, C.; Beams, R.; Novotny, L.; Vamivakas, A.N. Direct on-chip optical plasmon detection with an atomically thin semiconductor. *Nano Lett.* **2015**, *15*, 5477–5481. [[CrossRef](#)] [[PubMed](#)]
17. Suh, J.; Park, T.E.; Lin, D.Y.; Fu, D.; Park, J.; Jung, H.J.; Chen, Y.; Ko, C.; Jang, C.; Sun, Y.; et al. Doping against the native propensity of MoS₂: Degenerate hole doping by cation substitution. *Nano Lett.* **2014**, *14*, 6976–6982. [[CrossRef](#)] [[PubMed](#)]
18. Thakurta, S.R.G.; Dutta, A.K. Electrical conductivity, thermoelectric power and Hall effect in *p*-type molybdenite (MoS₂) crystal. *J. Phys. Chem. Solids* **1983**, *44*, 407–416. [[CrossRef](#)]
19. Fivaz, R.; Mooser, E. Mobility of charge carriers in semiconducting layer structures. *Phys. Rev.* **1967**, *163*, 743–755. [[CrossRef](#)]
20. Kim, S.; Konar, A.; Hwang, W.S.; Lee, J.H.; Lee, J.; Yang, J.; Jung, C.; Kim, H.; Yoo, J.B.; Choi, J.Y.; et al. High-mobility and low-power thin-film transistors based on multilayer MoS₂ crystals. *Nat. Commun.* **2012**, *3*, 1011–1017. [[CrossRef](#)] [[PubMed](#)]
21. Van Der Pauw, L.J. A method of measuring specific resistivity and Hall effect of discs of arbitrary shape. *Philips Tech. Rev.* **1958**, *20*, 220–224.
22. Park, K.T.; Babb, M.R.; Freund, M.S.; Weiss, J.; Klier, K. Surface structure of single-crystal MoS₂ (0002) and Cs/MoS₂ (0002) by X-ray photoelectron diffraction. *J. Phys. Chem.* **1996**, *100*, 10739–10745. [[CrossRef](#)]
23. Suzuki, R.; Sakano, M.; Zhang, Y.J.; Akashi, R.; Morikawa, D.; Harasawa, A.; Yaji, K.; Miyamoto, K.; Okuda, T.; Ishizaka, K.; et al. Valley-dependent spin polarization in bulk MoS₂ with broken inversion symmetry. *Nat. Nano Technol.* **2014**, *9*, 611–617. [[CrossRef](#)] [[PubMed](#)]
24. Andersen, A.; Kathmann, S.M.; Lilga, M.A.; Albrecht, K.O.; Hallen, R.T.; Mei, D. First-principles characterization of potassium intercalation in hexagonal 2H-MoS₂. *J. Phys. Chem. C* **2012**, *116*, 1826–1832. [[CrossRef](#)]
25. Wang, Q.H.; Kalantar-Zadeh, K.; Kis, A.; Coleman, J.N.; Strano, M.S. Electronics and optoelectronics of two-dimensional transition metal dichalcogenides. *Nat. Nano Technol.* **2012**, *7*, 699–712. [[CrossRef](#)] [[PubMed](#)]
26. Korona, K.P.; Wyszomolek, A.; Pakula, K.; Stepniewski, R.; Baranowski, J.M.; Grzegory, I.; Lucznik, B.; Wroblewski, M.; Porowski, S. Exciton region reflectance of homoepitaxial GaN layers. *Appl. Phys. Lett.* **1996**, *69*, 788–790. [[CrossRef](#)]
27. Xiao, D.; Liu, G.B.; Feng, W.; Xu, X.; Yao, W. Coupled spin and valley physics in monolayers of MoS₂ and other group-VI dichalcogenides. *Phys. Rev. Lett.* **2012**, *108*, 196802–196804. [[CrossRef](#)] [[PubMed](#)]
28. Varshni, Y.P. Temperature dependence of the energy gap in semiconductors. *Physica* **1967**, *34*, 149–154. [[CrossRef](#)]
29. O'Donnell, K.P.; Chen, X. Temperature dependence of semiconductor band gaps. *Appl. Phys. Lett.* **1991**, *58*, 2924–2926. [[CrossRef](#)]
30. Ho, C.H.; Wu, C.S.; Huang, Y.S.; Liao, P.C.; Tiong, K.K. Temperature dependence of energies and broadening parameters of the band-edge excitons of Mo_{1-x}W_xS₂ single crystals. *J. Phys. Condens. Matter.* **1998**, *10*, 9317–9328. [[CrossRef](#)]

